2020 IEEE 9th International Power Electronics and Motion Control Conference (IPEMC2020-ECCE Asia) | 978-1-7281-5301-8/20/$31.00 ©2020 IEEE | DOI: 10.1109/IPEMC-ECCEAsia48364.2020.9368095

Dynamic Response Improvement for DAB Converter with Constant Power Load under Extended-Phase-Shift Control Based on Trajectory Control

Mingkai Zheng, Huiqing Wen, Qinglei Bu, Haochen shi
Department of Electrical and Electronic Engineering
Xi'an Jiaotong-Liverpool University, 215123, Suzhou, China
E-mail: Mingkai.Zheng16@student.xjtlu.edu.cn; Huiqing.Wen@xjtlu.edu.cn

***Abstract*—Microgrid has been regarded by many researchers as the fundamental building block for the next generation power grid, where DC-DC converter plays a crucial role as the interface between main DC bus, energy generation facilities, and energy storage systems. Among many different topologies of DC-DC converters, bidirectional isolated dual-active-bridge (DAB) converter receives increasingly more attentions because of its many merits, including allowance on bidirectional power flow, isolation between power supply and load, and voltage level conversion. However, as the control scheme used to regulate DAB converter evolves, its output voltage and current could be roughly regarded as constant, which implies the converter actually feeds a constant power load (CPL). Nevertheless, because of its equivalent negative resistance effect, CPL could introduce instability to the system, causing output power to oscillate or drops to zero. This paper comprehensively explains the impact of this negative resistance effect, and, to cope with this problem, a nonlinear control method called trajectory control based on the natural switching surfaces (NSS) of DAB converter with extended-phase-shift (EPS) control will be derived. To better demonstrate the advantages of using trajectory control, a traditional linear controller, PI controller, is implemented as a comparison. Finally, by comparing the simulation results between traditional PI control and trajectory control, it is found that the start-up stage for trajectory control is much shorter than that of PI control, and the system stability of DAB converter feeding CPL is improved.**

***Index Terms*—Bidirectional full bridge DC-DC converter, trajectory control, Phase-shift control, Transient-state.**

I. Introduction

Dual-active-bridge (DAB) DC-DC converter plays a crucial role in the realization of distributed power system because of its many merits, including the bidirectional power flow between the source and loads, primary and secondary current isolation, and output voltage conversion by using phase-shift control [1–6]. For instance, in an electric vehicle system, DAB converters are usually used as the interface between the main DC bus and the energy storage system composed of batteries and supercapacitors. Compared to the traditional single-phase-shift (SPS) control, more advanced control strategies, such as extended-phase-shift (EPS) control, could improve overall system efficiency [7]. The circuit topology of DAB converter is illustrated in Fig. 1, where eight MOSFETs connected to the high frequency transformer, named from S_1 to S_8, are used to form isolation between primary side and secondary side, and inductor L represents the transformer leakage inductance [8–12].

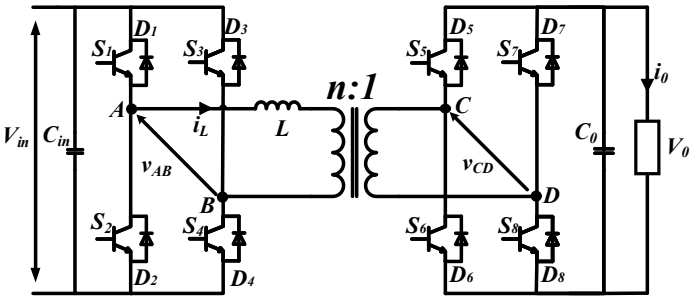

Fig. 1: Circuit topology for DAB converter

Constant power loads (CPL) have been found to be common in microgrid and electrical vehicle (EV) systems [13–16]. As the control methods on the converters evolves to achieve constant output current and voltage, their output power will roughly equal to constant [15]. Similarly, since the torque applied on a motor is constant under steady-state condition, if the speed of an EV is kept as approximately constant, it can also be regarded as a CPL [15].

Unlike the resistive load (RL), a spacial property of CPL, known as the dynamic negative resistance, introduces instability to the whole system. To cope with this issue, many methods have been proposed. For instance, in [14], a study has shown that traditional linear controller, is feasible to sustain the system stability by adding networks of passive components. However, the corresponding system efficiency and simplicity are sacrificed. A nonlinear control strategy called natural switching surfaces (NSS) has been proposed for DAB converter under EPS control [17], but the CPL condition was not mentioned.

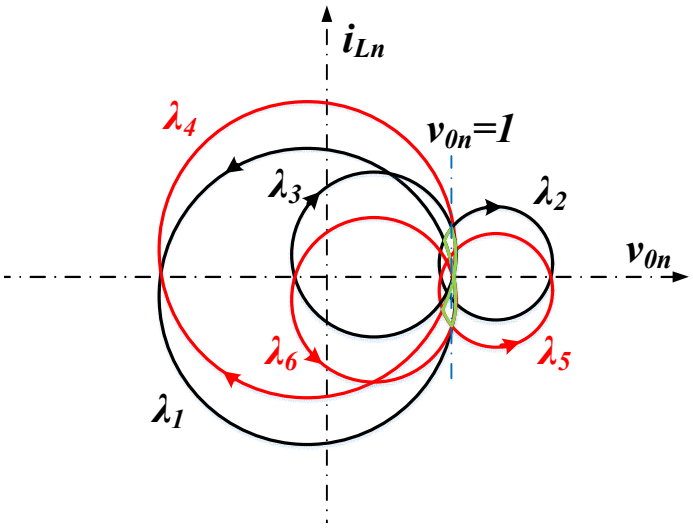

Fig. 2: NSS of DAB converter of buck mode

II. Constant Power Load with Trajectory Control

A. Constant power load characteristics

CPL phenomenon is common in mirogrid systems and electric vehicles. For instance, if the speed of a motor is tightly regulated with a constant torque, it will consume constant power (CP) [15]. Furthermore, when converters on loads of power system are tightly regulated, they can be regarded as CPLs as well [16]. Nonetheless, compared to the resistive load (RL) that has linear current-voltage relationship, CPL can introduce instability to a system because of its unique non-linear current-voltage relationship, which is also known as the negative resistance [13, 16]:

$$\frac{di_o}{dv_o} = \frac{d}{dv_o}\left(\frac{P_o}{v_o}\right) = -\frac{P_o}{v_o^2} = -\frac{1}{R_{CPL}}, \tag{1}$$

where P_o, v_o and i_o represent the output power, voltage and current, respectively.

B. Derivation of natural switching surface of DAB converter under EPS control

To derive the NSS of DAB converter under EPS control, its small-signal model based on the inductor current i_L and the ouput voltage v_0 would be necessary. According to the switching cases of EPS developed in [7], the inductor voltage v_L has six different values for EPS control of buck mode, which are $(V_{in}+v_0)$, $(V_{in}-v_0)$, $-v_0$, $(-V_{in}-v_0)$, $(-V_{in}+v_0)$, and v_0. The primary and secondary bridge voltage, v_{AB} and v_{CD}, can be written as $v_{AB} = s_1 V_{in}$ and $v_{CD} = s_2 V_0$, where $[s_1, s_2]$ have combinations as [1, -1], [1, 1], [0, 1], [-1, 1], [-1, -1], and [0, -1], corresponding to six different values of v_L, respectively.

Based on the small-signal model of DAB converter, the system could be represented by the following differential equations:

$$\begin{cases} \frac{dv_0}{dt} = \frac{1}{C_0}\left(s_2 i_L - i_0\right) \\ \frac{di_L}{dt} = \frac{1}{L}\left(s_1 V_{in} - s_2 v_0\right) \end{cases} \tag{2}$$

Define $V_{inn} = V_{in}/V_{ref}$, $v_{0n} = v_0/V_{ref}$, $i_{Ln} = i_L Z_0/V_{ref}$, $i_{0n} = i_0 Z_0/V_{ref}$, $Z_0 = \sqrt{L/C_0}$, $t_n = t f_n$, and $f_n = 1/(2\pi\sqrt{LC_0})$, the small-signal model with normalized system parameters can be expressed as [17]

$$\begin{cases} \frac{dv_{0n}}{dt_n} = 2\pi\left(s_2 i_{Ln} - i_{0n}\right) \\ \frac{di_{Ln}}{dt_n} = 2\pi\left(s_1 V_{inn} - s_2 v_{0n}\right) \end{cases} \tag{3}$$

Thus, by solving (3), the solution of the normalized inductor current i_{Ln} can be obtained,

$$\begin{aligned} i_{Ln} =& \left(i_{Ln}(0) - i_{0n}s_2\right)\cos(2\pi f_n t) \\ &+ \frac{1}{2\pi}\frac{di_{Ln}(0)}{dt_n}\sin(2\pi f_n t) + i_{0n}s_2, \end{aligned} \tag{4}$$

where $i_{Ln}(0)$ is the initial condition.

Based on this solution, the six trajectories of NSS of DAB converter under EPS control of buck mode could be expressed as

$$\begin{aligned} \lambda_{(1-6)} =& \left(V_{inn}s_1 - v_{0n}s_2\right)^2 - \left(i_{Ln\_(A-F)} - i_{0n}s_2\right)^2 \\ &- \left(V_{inn}s_1 - s_2\right)^2 + \left(i_{Ln} - i_{0n}s_2\right)^2 \end{aligned} \tag{5}$$

where each of the six trajectories of $\lambda_{(1-6)}$ corresponds to a circuit structure of six different modes, and $i_{Ln\_(A-F)}$ represent the reference values for inductor current i_{Ln} at steady-state operation for different NSS that are specified to stabilize the desired operation frequency. The equation that describes the trajectories in (5) are circles in state-space plane whose radii depend on the output current i_{0n}. Because i_{0n} merely has significantly small variations at steady-state operation, the radii of trajectories are regarded as constants. A conceptual diagram of trajectories in state-space plane of i_{Ln} versus v_{0n} is depicted in Fig. 2, where the trajectory of steady-state operation is in green.

C. Definition on the Control Strategy

The waveforms and trajectory of DAB converter with EPS control under steady-state operation are illustrated in more details in Figure 3. Since the DAB converter under steady-state operation with trajectory control and EPS control is directly equivalent to that under EPS control, $i_{L(A-F)}$ could be calculated by using time domain analysis [7]:

$$i_{L\_A} = -i_{L\_D} = \frac{V_{in}(2D_2 + D_1 - 1) + v_0}{4 f_s L} \tag{6}$$

$$i_{L\_B} = -i_{L\_E} = \frac{V_{in}(1 - D_1) + v_0(2D_1 + 2D_2 - 1)}{4 f_s L} \tag{7}$$

$$i_{L\_C} = -i_{L\_F} = \frac{V_{in}(1 - D_1) + v_0(2D_2 - 1)}{4 f_s L}. \tag{8}$$

where D_2 represents the phase shift between the primary side voltage v_{AB} and secondary side voltage v_{CD}, as it shown in Fig. 3(b). The name of this phase difference is based on the convention in [7], where the duty cycle of primary side voltage v_{AB} is defined as D_1 for EPS control. To calculate the

normalized values of $i_{L\_(A-D)}$, the following equation could be used:

$$i_{Ln} = \frac{i_L Z_0}{V_{ref}}. \tag{9}$$

The control scheme on the switching sequence for EPS control operating in buck mode is defined as: $\lambda_1 \rightarrow \lambda_2 \rightarrow \lambda_3 \rightarrow \lambda_4 \rightarrow \lambda_5 \rightarrow \lambda_6$. The switching actions from one state to another only occur if i_{Ln} reaches its target value. However, to avoid magnetic saturation on transformer, the magnitude of i_{Ln} should also be limited. So, switching actions could also occur if the customized limitations are reached. Because these limitations interfere the natural operation of trajectory control, it could result in having longer starting-up stage with more switching actions.

D. Intersections between RL and CPL trajectories

Considering CPL, the output current i_{0n} in (3) should be replaced by

$$i_{0n} = \frac{Z_0 P}{v_{0n} V_{ref}^2}, \tag{10}$$

where P is the target output power. The trajectories of CPL and NSS of six different modes are plotted in Fig. 4 with intersections labeled, which indicate where the switching actions occur if load is switched from RL to CPL and vice versa.

III. Simulation Results

To demonstrate the fast dynamic property of the proposed trajectory control, the simulation results of DAB converter under PI controller and trajectory control will be compared. The parameters of the components used are listed here: $V_{in} = 80$V, $V_0 = 40$V, $L = 150\mu$H, $C_{in} = C_0 = 200\mu$F, and the transformer turns ratio is 1:1.

With the phase shift $D_1 = 0.1$, the simulation results of DAB converter with PI controller is illustrated in Fig. 5, where, in Fig. 5(a), the step signal represents when the load is changed from 50W RL to 125W CPL. The time span for the start-up stage is approximately 7ms, and, after the load being changed from RL to CPL at 8ms, it fails to sustain the stability, and the output voltage V_0 gradually decreases to 0. Finally, the output power equals to zero. In contrast, as the simulation results of DAB converter with trajectory control shown in Fig. 6, it only takes less than 1.5ms to complete the start-up stage, which reveals the fast dynamic property of trajectory control. Moreover, after the load being switched from 50W RL to 125W CPL, the system stability is sustained. Additionally, from the state-space plot in Fig. 6(b), the trajectory control limits the trajectory of DAB converter of steady-state operation to a dramatically small region, which implies small output voltage ripple. Consequently, it has been proved that the dynamic performance and system stability of DAB converter under EPS control could be improved by using trajectory control .

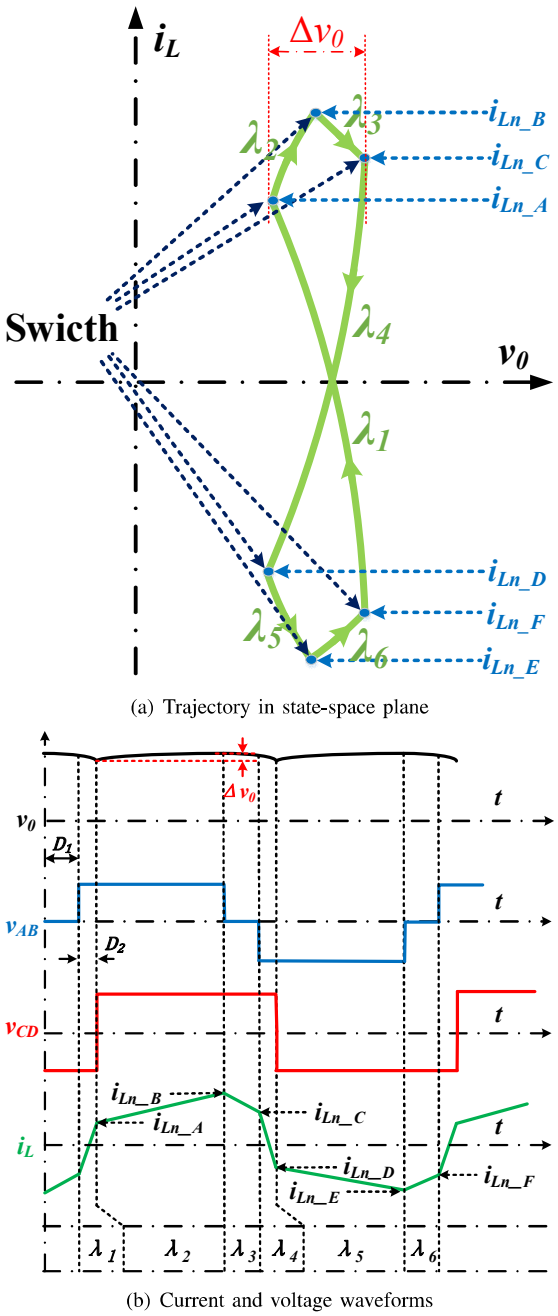

(a) Trajectory in state-space plane

(b) Current and voltage waveforms

Fig. 3: DAB converter with EPS control under steady-state operation

IV. Conclusion

In conclusion, this paper has demonstrated the derivation of NSS equations of DAB converter under EPS control. By comparing to the use of traditional PI controller, the fast dynamic response property of trajectory control for DAB converter under EPS control, especially the time span of the start-up stage, have been validated. In addition, it has been noticed that this control strategy can also improve the system stability and reduce steady-state voltage ripple.

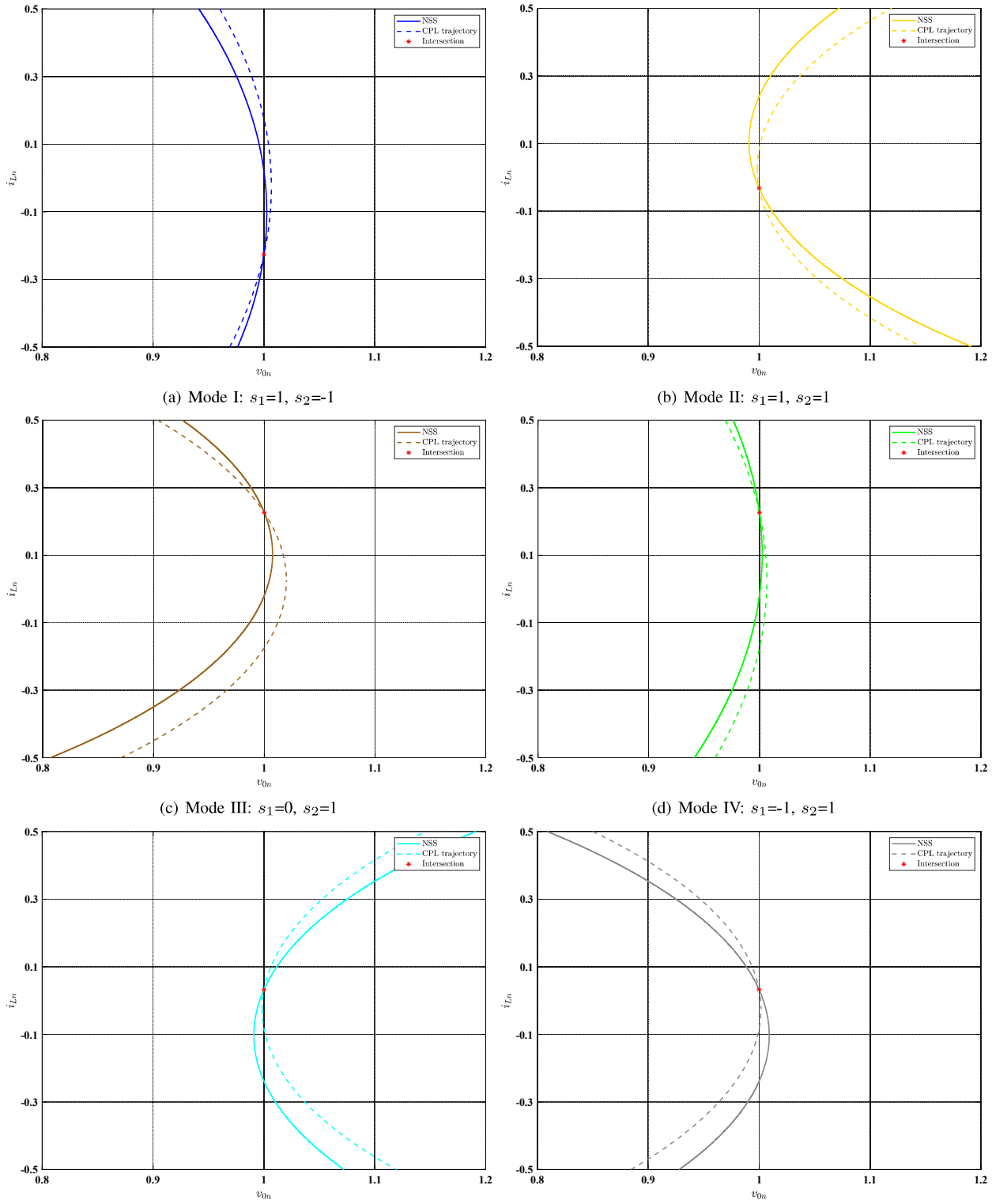

(a) Mode I: s_1=1, s_2=-1

(b) Mode II: s_1=1, s_2=1

(c) Mode III: s_1=0, s_2=1

(d) Mode IV: s_1=-1, s_2=1

(e) Mode V: s_1=-1, s_2=1

(f) Mode VI: s_1=0, s_2=-1

Fig. 4: NSS and CPL trajectories under different circuit structures of EPS

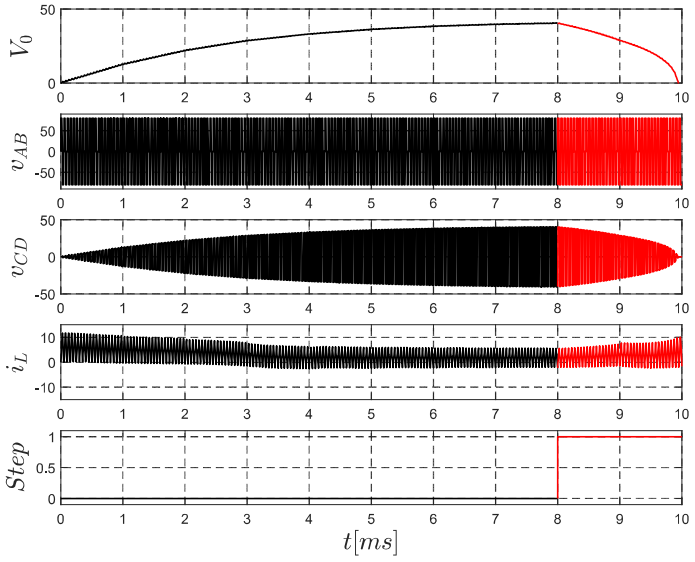

(a)

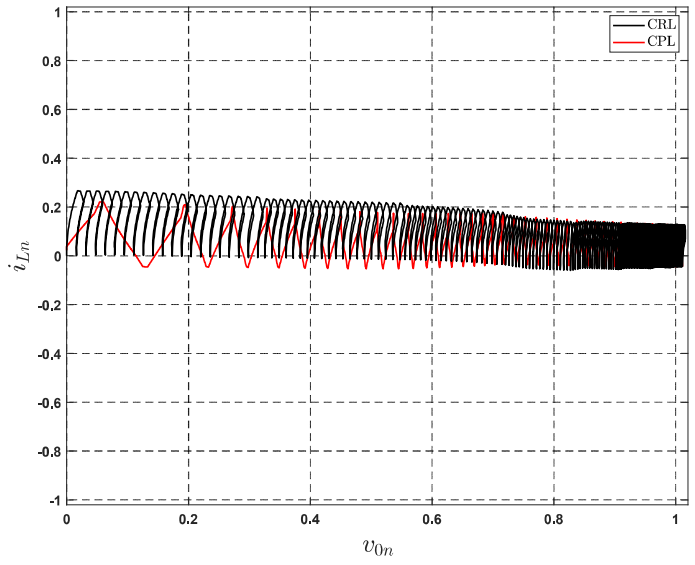

(b)

Fig. 5: Simulation results of DAB converter of PI control with load being switched from RL to CPL at 8 ms. (a) Waveforms of output voltage V_0, the primary bridge voltage v_{AB}, the secondary bridge voltage v_{CD}, inductor current i_L, and the switching signal (Step). (b) The state-space plane of v_{0n} versus i_{Ln}.

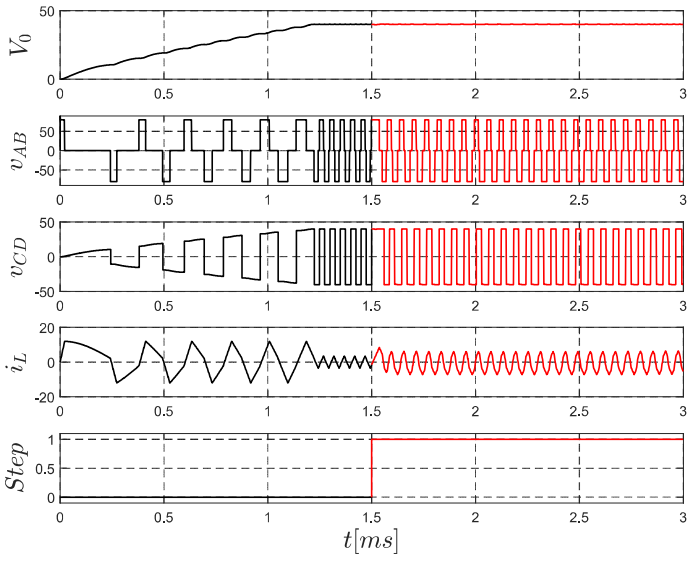

(a)

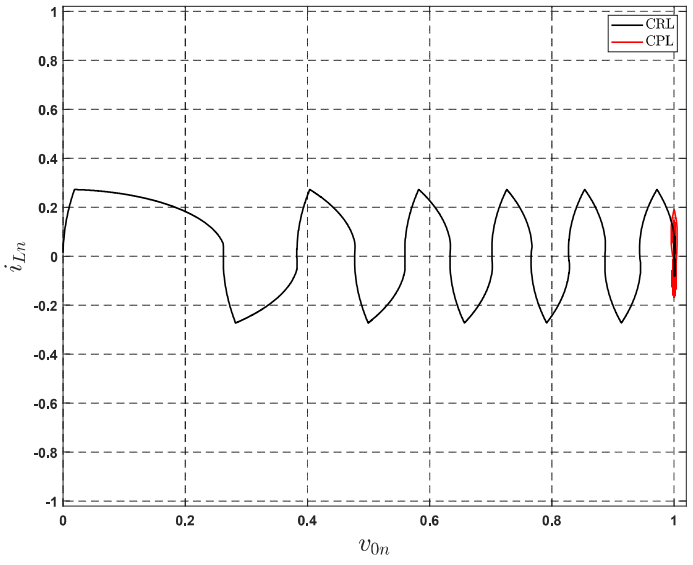

(b)

Fig. 6: Simulation results of DAB converter of trajectory control, switching from RL to CPL at 1.5 ms. (a) Waveforms of output voltage V_0, the primary bridge voltage v_{AB}, the secondary bridge voltage v_{CD}, inductor current i_L, and the switching signal (Step). (b) The state-space plane of v_{0n} versus i_{Ln}.

V. Acknowledgement

This work was supported by the Research development fund of XJTLU (RDF-16-01-10, RDF-17-01-28), the Research Enhancement fund of XJTLU (REF-17-01-02), the Suzhou Prospective Application programme (SYG201723), and the XJTLU Key Programme Special Fund (KSF-A-08, KSF-E-13KSF-T-04).

References

[1] C. A. Hill, M. C. Such, D. Chen, J. Gonzalez, and W. M. Grady, "Battery Energy Storage for Enabling Integration of Distributed Solar Power Generation," *IEEE Trans. Smart Grid*, vol. 3, no. 2, pp. 850–857, June 2012.

[2] P. Xia, H. Shi, H. Wen, Q. Bu, Y. Hu, and Y. Yang, "Robust lmi-lqr control for dual-active-bridge dcdc converters with high parameter uncertainties," *IEEE Transactions on Transportation Electrification*, vol. 6, no. 1, pp. 131–145, 2020.

[3] H. Shi, H. Wen, and Y. Hu, "Deadband effect and accurate zvs boundaries of gan-based dual-active-bridge converters with multiple-phase-shift control," *IEEE Trans-*

actions on Power Electronics, vol. 35, no. 9, pp. 9888–9905, 2020.

[4] P. Thounthong, "Model Based-Energy Control of a Solar Power Plant With a Supercapacitor for Grid-Independent Applications," *IEEE Transactions on Energy Conversion*, vol. 26, no. 4, pp. 1210–1218, Dec 2011.

[5] Q. Bu, H. Wen, J. Wen, Y. Hu, and Y. Du, "Transient dc bias elimination of dual active bridge dc-dc converter with improved triple-phase-shift control," *IEEE Transactions on Industrial Electronics*, pp. 1–1, 2019.

[6] W. Jing, C. Hung Lai, S. H. W. Wong, and M. L. D. Wong, "Battery-supercapacitor hybrid energy storage system in standalone DC microgrids: a review," *IET Renewable Power Generation*, vol. 11, no. 4, pp. 461–469, 2017.

[7] B. Zhao, Q. Yu, and W. Sun, "Extended-Phase-Shift Control of Isolated Bidirectional DCDC Converter for Power Distribution in Microgrid," *IEEE Trans. Power Electron.*, vol. 27, no. 11, pp. 4667–4680, Nov 2012.

[8] M. Farhangi, W. Xiao, and H. Wen, "Advanced modulation scheme of dual active bridge for high conversion efficiency," in *2019 IEEE 28th International Symposium on Industrial Electronics (ISIE)*, 2019, pp. 1867–1871.

[9] H. Wen and Z. Cao, "Affine parameterization for the dual phase-shifted bidirectional isolated dc-dc converters," in *2018 IEEE International Conference on Power Electronics, Drives and Energy Systems (PEDES)*, 2018, pp. 1–6.

[10] Q. Bu and H. Wen, "Triple-phase-shifted bidirectional full-bridge converter with wide range zvs," in *2018 IEEE International Conference on Power Electronics, Drives and Energy Systems (PEDES)*, 2018, pp. 1–6.

[11] H. Shi, H. Wen, and Z. Cao, "Optimal minimized reactive power boundary control based on the six natural switching surface," in *2018 IEEE International Conference on Power Electronics, Drives and Energy Systems (PEDES)*, 2018, pp. 1–6.

[12] H. Wen and L. Zheng, "Minimum backflow power control of bidirectional isolated dc-dc converters," in *2018 IEEE International Conference on Power Electronics, Drives and Energy Systems (PEDES)*, 2018, pp. 1–5.

[13] A. Emadi, A. Khaligh, C. H. Rivetta, and G. A. Williamson, "Constant power loads and negative impedance instability in automotive systems: definition, modeling, stability, and control of power electronic converters and motor drives," *IEEE Trans. Veh. Technol.*, vol. 55, no. 4, pp. 1112–1125, July 2006.

[14] A. M. Rahimi and A. Emadi, "An Analytical Investigation of DC/DC Power Electronic Converters With Constant Power Loads in Vehicular Power Systems," *IEEE Trans. Veh. Technol.*, vol. 58, no. 6, pp. 2689–2702, July 2009.

[15] Y. A. I. Mohamed, A. A. A. Radwan, and T. K. Lee, "Decoupled reference-voltage-based active dc-link stabilization for pmsm drives with tight-speed regulation," *IEEE Trans. Ind. Electron.*, vol. 59, no. 12, pp. 4523–4536, Dec 2012.

[16] D. P. Ariyasinghe and D. M. Vilathgamuwa, "Stability analysis of microgrids with constant power loads," in *2008 IEEE International Conference on Sustainable Energy Technologies*, Nov 2008, pp. 279–284.

[17] G. G. Oggier and M. Ordonez, "High-Efficiency DAB Converter Using Switching Sequences and Burst Mode," *IEEE Trans. Power Electron.*, vol. 31, no. 3, pp. 2069–2082, March 2016.